A visible light driven photocatalytic removal of water pollutants by carbon modified magnetically active ternary TiO$_2$ (Fe$_3$O$_4$/Carbon/TiO$_2$) composite

Rajakumar Ananthakrishnan[*a] and Priyanka Das[a]

[a]Department of Chemistry, Environmental Materails & Analytical Chemistry Laboratory,

Indian institute of technology, Kharagpur 721302, India

*Corresponding author email: raja.iitchem@yahoo.com

SUPPORTING INFORMATION:

Synthesis of Fe$_3$O$_4$/C/TiO$_2$ with different ratio:

A new series of catalysts with variation in the ratios of its components were prepared by using the similar hydrothermal method described above. FCT-500 was taken as standard and the amount of TiO$_2$ (x in FCT) and amount of carbon (y in FCT) are varied in the respective steps mentioned earlier. All the catalysts were calcined at 500°C and named as FCT(0.5x), FCT(2x), FC(0.0y)T, FC(0.5y)T and FC(2y)T accordingly.

Structural and morphological studies of FCT with different ratio in compositions:

On varying the composition ratio, the peaks for both Fe$_3$O$_4$ and TiO$_2$ are retained with different crystallite size in the PXRD patterns of all the altered materials (Fig. S1a). No significant peak for carbon even on increasing the carbon content confirms the amorphous nature of carbon in these composites.

The UV-Vis diffusion reflectance spectra of as-prepared composites with different ratio in components are compared in Fig. S1b. The materials absorb in same region of visible light as previous, though the intensity of absorbance is different in case of changing the ratios.
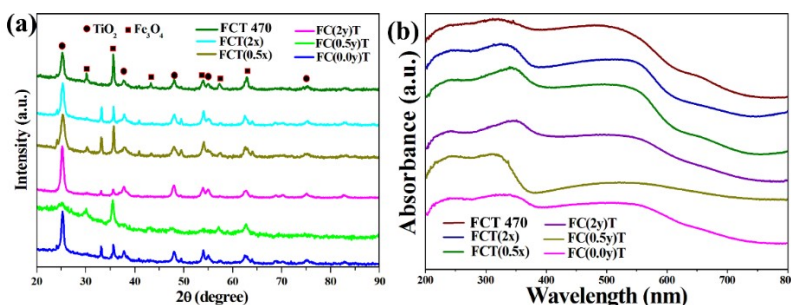

Fig. S1. (a) PXRD patters of FCT with different ratios in composition, (b) Absorption spectra of different composition of FCT.
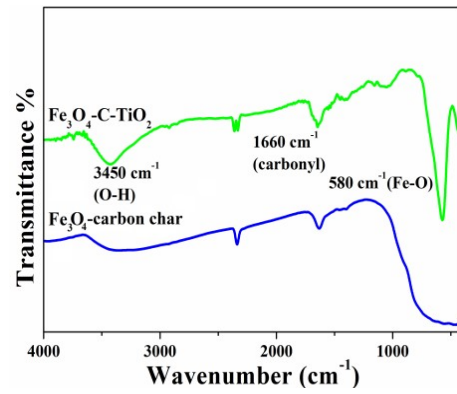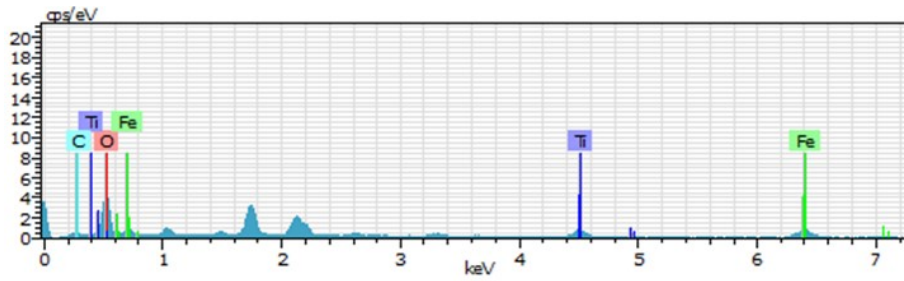
Fig. S2. FTIR spectra of FCT and Fe$_3$O$_4$-carbon.

Fig. S3. EDX spectrum of FCT
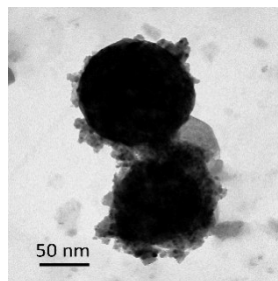

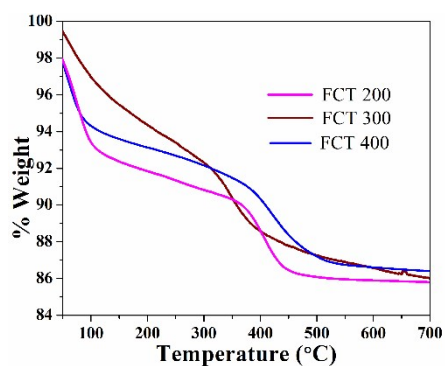**Figure S4**. TEM image of Fe$_3$O$_4$/carbon (500 °C).

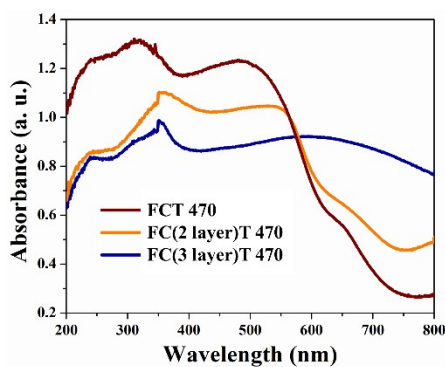**Fig. S5**. TGA of FCT 200, FCT 300 and FCT 400

Fig. S6. DRS spectra of FCT with difference in carbon layer by repeated hydrothermal.
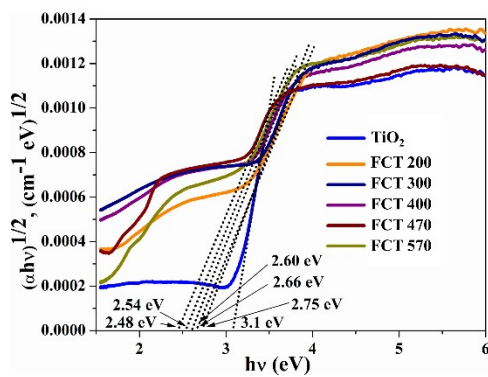

Fig. S7. Band gap values from Tauc plot of TiO_2 and FCT composites calcined at different temperature.

Mott-Schottky characterization:

using CHI 760D electrochemical workstation (CH Instruments, Inc., USA) using a three-electrode configuration in 0.5 M Na_2SO_4 electrolyte. The catalyst-coated fluorine doped tin oxide (FTO) glass substrate, Pt wire, and saturated calomel electrode (SCE) were used as working, counter, and reference electrode, respectively. The Mott–Schottky plots of the photocatalyst FCT 500 and TiO_2 were obtained by using Equation 1:

$$\frac{1}{C^2} = \frac{2}{q\varepsilon\varepsilon_0 N_D}(E - E_{fb} - \frac{KT}{q})$$
(1)

where C is the space-charge capacitance, ε the dielectric constant of material, ε_0 the permittivity of vacuum (8.85×10^{-14} Fcm^{-2}), q the charge of an electron and N_D the donor density of the semiconductor; E, E_{fb}, k and T are applied potential, flat-band potential, Boltzmann constant and absolute temperature, respectively. [Pradhan *et al*., doi.org/10.1002/cssc.202000308] The obtained plot (given below) show positive slope indicating n-type nature of semiconductor. The flat band potential shifted to more negative value (-0.52 V) for the ternary hybrid from that of pristine TiO_2. The conduction band (E_{CB}) and valance band (E_{VB}) potential of the heterojunction hybrid are calculated using the equations 2 and the band gap value obtained from DRS (2.48 eV):

$$E_{CB} \text{ (NHE, pH 7)} = E_{fb} \text{ (SCE, pH 7)} + 0.04$$
(2)

The CB/VB positions were calculated as -0.47 V/2.01 V for the heterostucture. To explain the photocatalysis process different control experiments were done to find that hydroxyl radical, superoxide radical and holes are responsible for degrading the reactant. The electrons exited on irradiation to conduction band of TiO_2 can drive to Fe_3O_4 via carbon layer, where Fe(II) and Fe (III) can interchange to provide the electron for formation of superoxide radical ($O_2^{\cdot-}$) from atmospheric O_2. On the other hand, the holes in valance band of TiO_2 can be involved in producing hydroxyl radical (OH·).
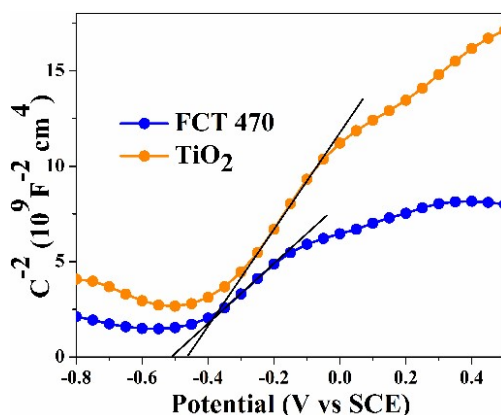

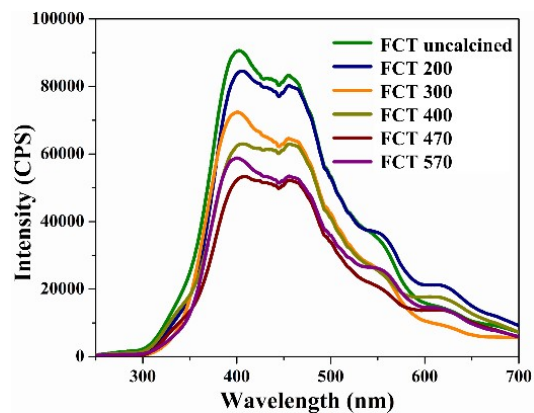**Fig S8**. Mott-Schottky plots for TiO_2 and FCT 470

Fig. S9. PL spectra of $Fe_3O_4/C/TiO_2$ composite prepared at different temperatures.
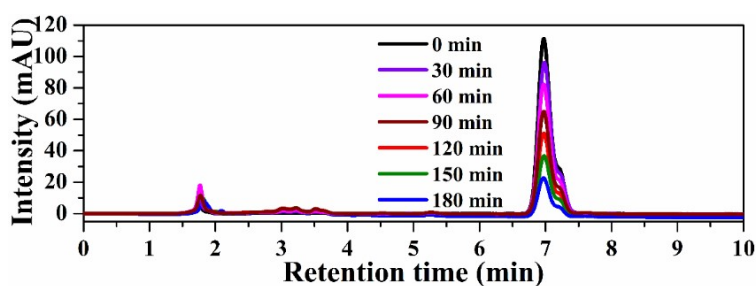

Fig. S10. HPLC chromatogram for degradation of BPA at different time interval;

HPLC conditions: run time – 10 min, mobile phase – Water:CH_3CN = 40:60, flow rate – 0.3 ml/min
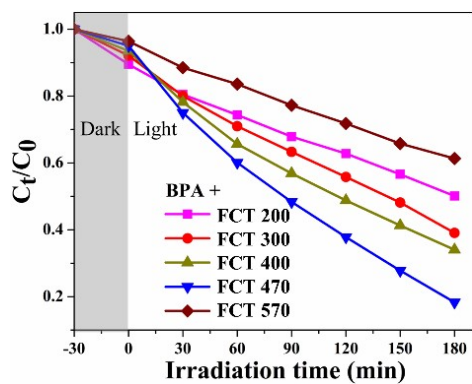

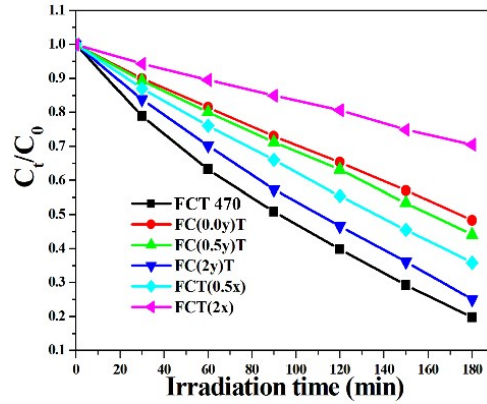**Fig. S11.** Photocatalytic degradation of BPA along with adsorption in dark before irradiation.

5

Fig. S12. Kinetic study for photocatalytic activity of FCT (with a change in component ratio).
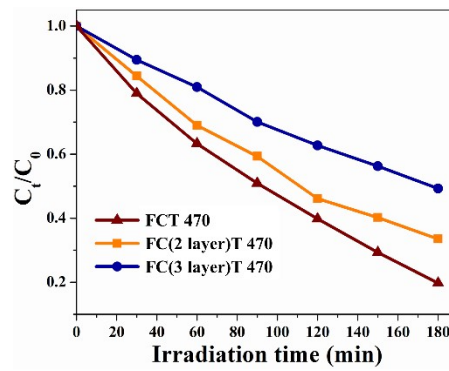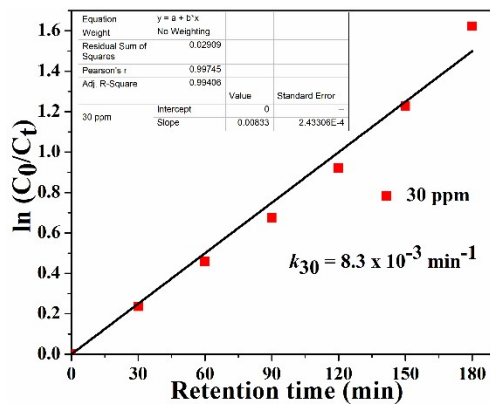

Fig. S13. Kinetic study for photocatalytic activity of FCT with different layers of carbon.

Assuming the Langmuir–Hinshelwood model for the photocatalytic reaction, the rate equation is as follows:

$r = -dc/dt = kKc/(1 + Kc)$

Taking Kc <<1 and integrating, the equation is

$\ln(C_0/C_t) = kKt = k't$

Fig. S14. Kinetics of BPA degradation using FCT 470.

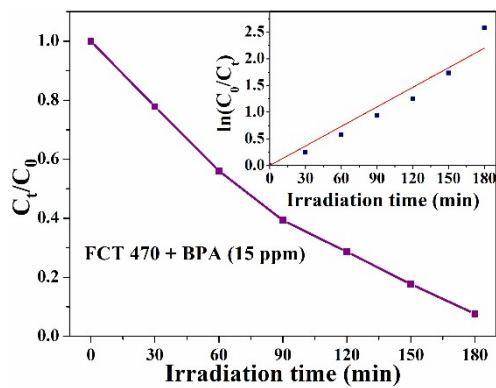**Fig. S15**. Degradation kinetics of 15 ppm BPA with FCT 470 (1 g L^{-1}); k_{15} = 13 x 10^{-2} min^{-1}
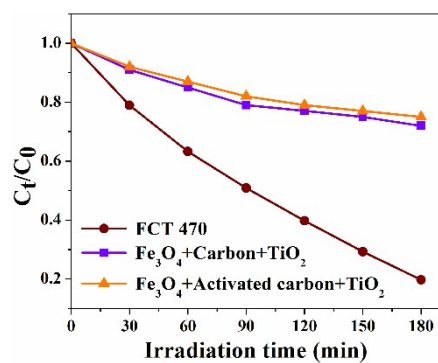
Figure S16. Photocatalytic activity of FCT 470 and physical mixture of metal oxides with carbon from D-gluconic acid and activated carbon separately.
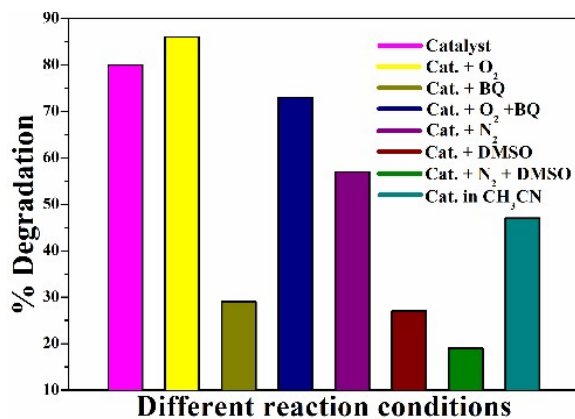
Fig. S17. Percentage for degradation of BPA using FCT 470 in presence of scavengers and gases.
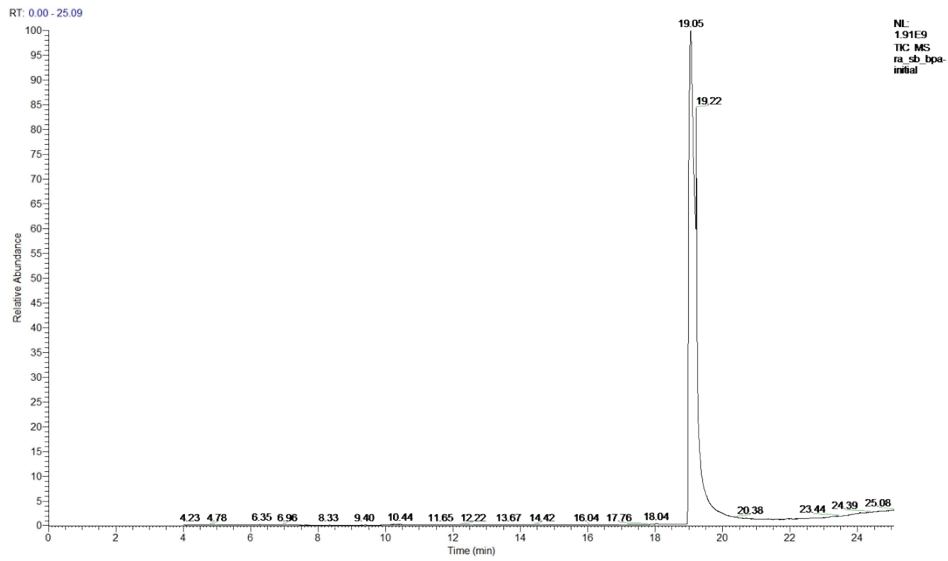
Fig. S18. Chromatogram for initial BPA solution obtained from GC.
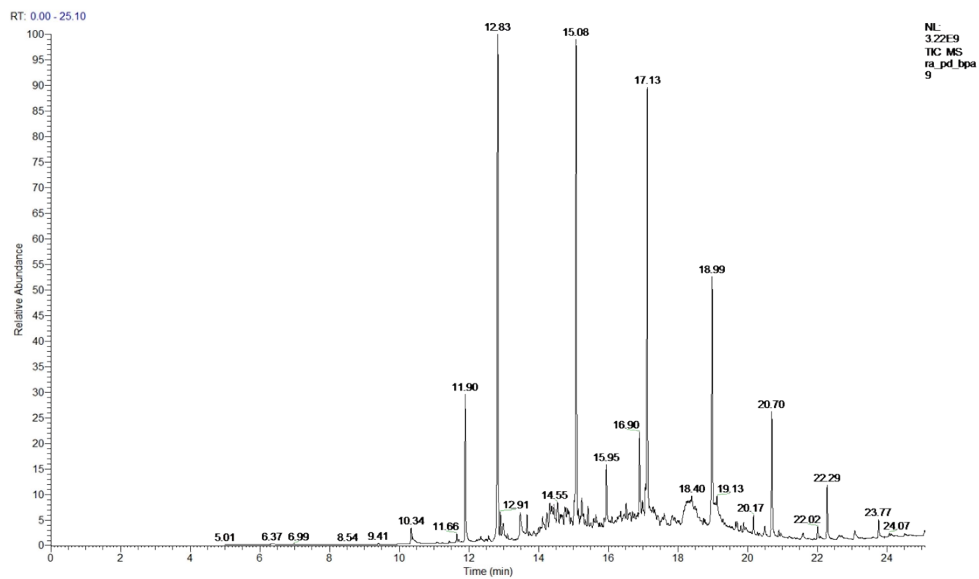
Fig. S19. GC chromatogram of the reaction mixture taken at 60 min of reaction.

(a) 11.9 min

m/z = 191

(b) 12.83 min

m/z = 139

(c) 16.9 min

m/z = 149 min

(d) 19.13 min

m/z = 229

(e) 22.29 min

m/z = 283
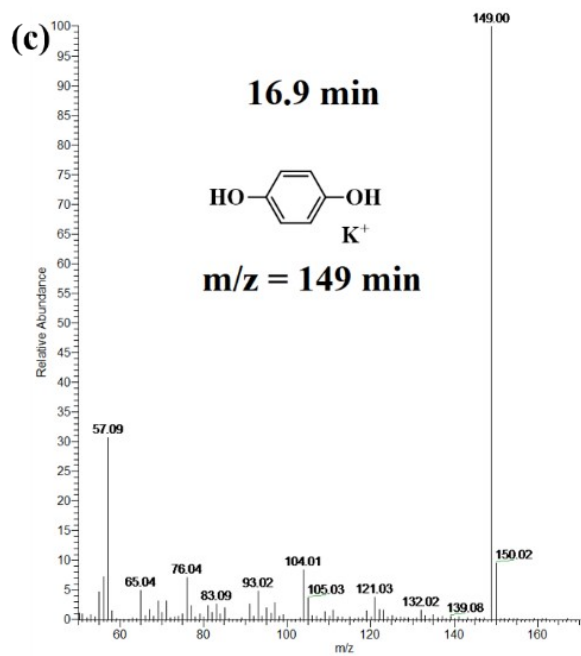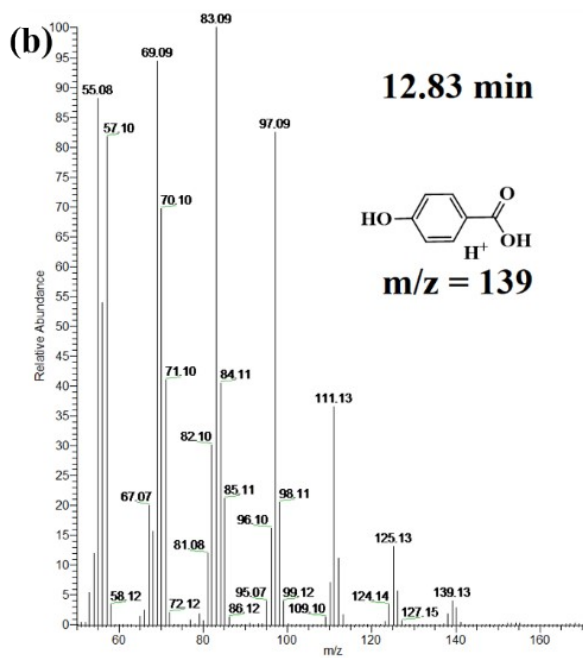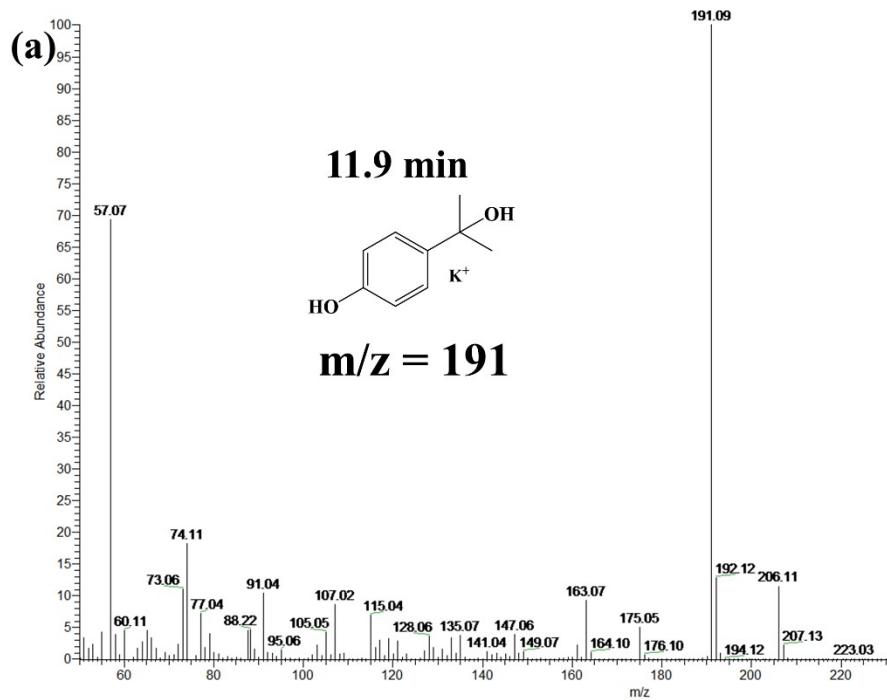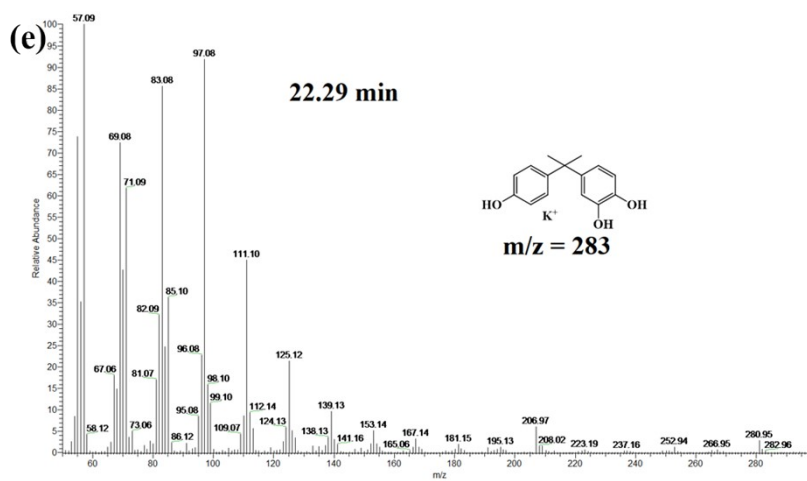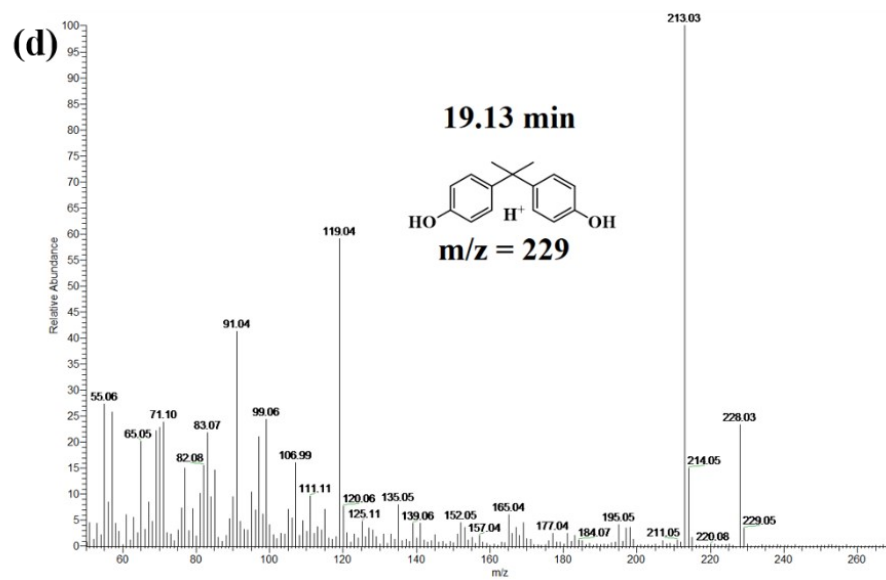
Fig. S20a-e. GCMS profile for different retention times for reaction mixture taken at 60 min of reaction.

Fig. S21. Magnetically active composite
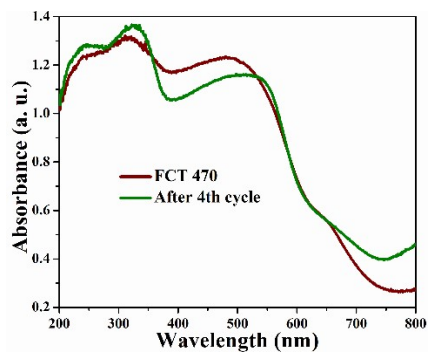
Fig. S22. UV-Vis reflectance spectra of the fresh and reused catalysts.

Fig. S23. PXRD pattern of the fresh and reused catalysts.

Table S1. Surface area of composites obtained from BET isotherm

Composite	Surface area (m^2/g)
Fe_3O_4	90
Fe_3O_4-C (uncalcined)	273
Fe_3O_4/TiO_2 (470 °C)	51
$Fe_3O_4/C/TiO_2$ (470 °C)	73

Table S2. Comparison of photocatalytic efficiency of composite with reported literatures

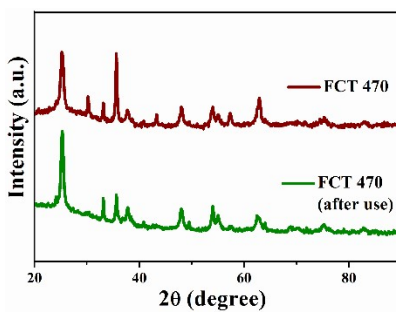| Catalysts	Application	Pollutant Conc. Catalyst dose	Light source	%Deg.	Rate constant (min^{-1})	Ref.
Fe^{3+} doped TiO_2	Malachite Green	2.5 mg L^{-1} Coated glass plates	8W UV light	85%	0.0202	[1]
$TiO_2@Fe_3O_4$-carbon	teracycline	20 ppm Cat. 1 gL^{-1}	350 W Xe lamp	82.6%	-	[2]
Fe_3O_4/CRC	Cu(II) removal	10 ppm Cat. 0.2 gL^{-1}	Adsorption	44.96 mg g-1	0.0904 g mg^{-1} min^{-1}	[3]
AgInSe$_2$/TiO$_2$	MB MO RhB	100 ppm Cat. 2 gL^{-1}	8 W UV lamp	87% 83% 52%	0.1067 0.1136 0.1028	[4]
Fe$_3$O$_4$@TiO$_2$	Bisphenol A	0.088 mM Cat. 1.5 g L^{-1}	UV lamp (λ=254 nm)	~90%	0.242 (with H$_2$O$_2$)	[5]
Iron Oxide/MWCNT /Ag-doped TiO$_2$	Phenol	50 ppm Cat. 300 mg	UV-Vis (λ > 300 nm)	85% TOC removal and 100 % removal of phenol	0.0255	[6]
α-Fe$_2$O$_3$ Nanoparticles	Atrazine (ATZ) Rhodamine B (RhB)	5 ppm (RhB) 2.5 ppm (ATZ) Cat. 0.1 gL^{-1}	UVC lamp 15 W	40 % and 59 % of RhB and ATZ in 40 min	-	[7]
N, Co Codoped TiO$_2$	Bisphenol A	30 ppm Cat. 140 mg L^{-1}	Solar light UV	98%	0.0195	[8]
Activated carbon/TiO$_2$	Bisphenol A	- Cat. 0.1 gL^{-1}	150 W mercury lamp	90%	0.078	[9]
Fe$_3$O$_4$-C-TiO$_2$	Bisphenol A	15 ppm 1 gL^{-1}	250 W Tungsten lamp	95%	0.13	Our work

Catalyst	Degradation of Rhodamine B	Light Source	Rate constant	Degradation % (min)	Reference
C-TiO$_2$	RhB conc. 5 ppm Cat. dose 1 g L^{-1}	500 W tungsten halogen lamp	0.01061 min^{-1}	85% 60 min	[10]
Fe$_3$O$_4$/C (Photo-Fenton)	RhB conc. ~5 ppm Cat. dose 0.5 g L^{-1}	100 W Xenon lamp	0.01779 min^{-1}	96% 180 min	[11]
Fe$_3$O$_4$	RhB conc. 10 ppm Cat. dose 1 g L-1	Visible light ($\lambda \geq 420$ nm)	0.0322 min^{-1}	97 % 80 min	[12]
Fe$_3$O$_4$@SiO$_2$@TiO$_2$/GO	RhB conc. ~10 ppm Cat. dose 1 g L^{-1}	400 W high-pressure mercury lamp	0.0136 min^{-1}	92.03% 150 min	[13]
Ag/r-GO/TiO$_2$	RhB conc. 10 ppm Cat. dose 0.5 g L^{-1}	150 W Xe lamp	0.0217 min^{-1}	80% 160 min	[14]
Fe$_3$O$_4$/C/TiO$_2$	RhB conc. 10 ppm Cat. dose 1 g L^{-1}	250 W Tungsten lamp	0.0358 min^{-1}	97% 90 min	Our work

Table S3: Comparison of degradation of rhodamine B with literature

References:

1   M. Asiltürk, F. Sayılkan and E. Arpaç, *J. Photochem. Photobiol. A Chem.*, 2009, **203**, 64–71.

2   X. Zhao, Z. Lu, J. Kan, C. Yi, N. Gao, Z. Zhu, M. Song, Y. Yan, Y. Wang and T. Zhang, *RSC Adv.*, 2016, **6**, 46889–46899.

3   L. Qu, J. Jia, H. Shi and Z. Luo, *New J. Chem.*, 2016, **40**, 2895–2903.

4   A. S. Kshirsagar and P. K. Khanna, *Inorg. Chem. Front.*, 2018, **5**, 2242–2256.

5   J. C. and J. K. Xingxing Li, Mingcan Cui, Yonghyeon Lee, *RSC Adv*, 2019, **9**, 22153–22160.

6   J. Marques Neto, C. Bellato, C. de Souza, R. da Silva and P. Rocha, *J. Braz. Chem. Soc.*, 2017, **28**, 2301–2312.

7   M. Rincón Joya, J. Barba Ortega, J. O. D. Malafatti and E. C. Paris, *ACS Omega*, 2019, **4**, 17477–17486.

8   A. Garg, T. Singhania, A. Singh, S. Sharma, S. Rani, A. Neogy, S. R. Yadav, V. K. Sangal and N. Garg, *Sci. Rep.*, 2019, **9**, 1–13.

9   P. Zawadzki, E. Kudlek and M. Dudziak, *J. Ecol. Eng.*, 2018, **19**, 260–268.

10   Y. Yuan, X. Qian, H. Han and Y. Chen, *J. Mater. Sci. Mater. Electron.*, 2017, **28**, 10028–10034.

11   M. Periyasamy, S. Sain, U. Sengupta, M. Mandal, S. Mukhopadhyay and A. Kar, *Mater. Adv.*, 2021, **2**, 4843–4858.

12   I. N. Reddy, A. Sreedhar, C. V. Reddy, J. Shim, M. Cho, D. Kim, J. S. Gwag and K. Yoo, *J. Solid State Electrochem.*, 2018, **22**, 3535–3546.

13   F. Chen, F. Yan, Q. Chen, Y. Wang, L. Han, Z. Chen and S. Fang, *Dalt. Trans.*, 2014, **43**, 13537–13544.

14   W. Gao, M. Wang, C. Ran, X. Yao, H. Yang, J. Liu, D. He and J. Bai, *Nanoscale*, 2014, **6**, 5498.